Proceedings of the Project Review, Geo-Mathematical Imaging Group (Purdue University, West Lafayette IN), Vol. 1 (2009) pp. 157-164.

MIGRATION VELOCITY ANALYSIS USING WAVE PACKETS - GEOMETRIC APPROACH *

ANTON A. DUCHKOV†, MAARTEN V. DE HOOP‡, AND FREDRIK ANDERSSON§

Abstract. Current algorithms for imaging seismic reflection data can be subdivided into two classes: Kirchhoff (generalized Radon transform) and wave-equation (double-square-root and reverse-time) migration. Kirchhoff type methods rely on asymptotic and ray-geometrical considerations. Wave-equation imaging algorithms (one-way or two-way) appear to be more robust in the case of complicated velocity models and aim to account for finite-frequency effects. Integration of the two classes, using wave packets or "curvelets", for the purpose of migration velocity analysis is the subject of this paper. One can represent full wave-form data in terms of wave packets with arbitrary accuracy on the one hand. On the other hand, every packet is characterized by a central point and direction that provides geometrical information that can be further utilized in "ray"-geometrical analysis, which is exploited, here, in the context of reflection tomography using annihilators derived from the wave-equation angle transform.

Key words. velocity continuation, angle transform, curvelet transform

AMS subject classifications.

1. Introduction. It is a well-known feature of seismic data and seismic images that signals are concentrated along piece-wise smooth hypersurfaces (traveltime surfaces in the data and interfaces in the (extended) image). Points on these surfaces are tied to orientations ((co)normal vectors). This information is indirectly used in Kirchhoff migration as a constructive summation principle. Local slant stack analysis has been used to reveal orientations present in the data, which, in turn, have been utilized in, for example, parsimonious migration [13], map migration [14], etc.; for a more complete list of references, see [4]. Goldin [10, 11] used contact elements to describe the propagation of singularities by migration-demigration. Here, we use elements of symplectic geometry instead.

Wave packets have been used to construct parametrices of the wave and evolution equations [18, 1]. The concentration of wave packets replaces the notion of propagation of singularities in the microlocal point of view. Evolution equations describe the continuation of initial data with respect to an evolution parameter. Examples include downward continuation (using the double-square root (DSR) equation) and velocity continuation; for a more detailed discussion see [7].

Wave packets, and the frames they form, are derived from the so-called dyadic parabolic decomposition of phase space. Different discretizations include the "curvelets" [2] and the discrete, almost symmetric wave packets [1]. The associated transforms yields sparse representations of seismic data and images, and replace the above mentioned naive local slant stack analysis. The decompositions into wave packets also appear to be a powerful tool for compressing, denoising, interpolating and regularizing seismic data or images [5, 12].

One can represent full wave-form data in terms of wave packets with arbitrary accuracy on the one hand. On the other hand, every packet is characterized by a central point and direction that provides geometrical information that can be further utilized in "ray"-geometrical analysis, which is exploited, here, in the context of reflection tomography using annihilators derived from the wave-equation angle transform.

2. Angle transform and velocity continuation.

2.1. Angle transform and common-image point gathers. To express redundancy in seismic reflection data, d, we use the so-called angle transform, $\mathcal{A}_{we}$, defined in [21]. This transform

*This research was supported in part under NSF CMG grant DMS 0724644, and by the members of the Geo-Mathematical Imaging Group (ExxonMobil, Total, BP, Statoil, ConocoPhillips).

†Center for Computational and Applied Mathemematics, and Geo-Mathematical Imaging Group, Purdue University, West Lafayette, IN 47907, USA (aduchkov@purdue.edu).

‡Center for Computational and Applied Mathemematics, and Geo-Mathematical Imaging Group, Purdue University, West Lafayette, IN 47907, USA (mdehoop@purdue.edu).

§Centre for Mathematical Sciences, Lund University, Box 118, SE-22100, Lund, Sweden.

is dependent on the background, velocity model, c; here, we consider a one-parameter family of such background models, $c(\alpha)$. Each model $c(\alpha)$ defines an angle transform $\mathcal{A}_{we}(\alpha)$. We have

$$\mathcal{A}_{we}(\alpha):\ d(\mathbf{x}_s,\mathbf{x}_r,t)\to w(\alpha,\mathbf{x},\mathbf{p},z), \tag{2.1}$$

where the $w(\alpha,\mathbf{x},\mathbf{p},z)$ are referred to as common-image point gathers (CIGs). (The term CIG is conventially reserved for w with $\mathbf{x}$ fixed.) Asymptotically, w recovers the singularities of the contrast (reflectivity); $\mathbf{p}$ is related to the scattering angle and azimuth (in 3D) of reflection, and can be viewed as a semblance parameter.

The particular angle transform used in this paper, is composed of data downward continuation and certain beamforming. In [21] it was shown that under mild conditions (essentially rays being nowhere "horizontal") the angle transform $\mathcal{A}_{we}$ is microlocally invertible. For the "true" background model, $w(\alpha,\mathbf{x},\mathbf{p},z)$ is independent of $\mathbf{p}$, which is exploited in designing an error criterion for background velocity estimation.

2.2. Velocity continuation of common-image point gathers. Assuming invertibility of $\mathcal{A}_{we}(\alpha)$ for all α in an interval of interest, we define a velocity continuation operator for common-image point gathers according to

$$C_{(\alpha,\alpha_0)}=\mathcal{A}_{we}(\alpha)\mathcal{A}_{we}^{-1}(\alpha_0); \tag{2.2}$$

$C_{(\alpha,\alpha_0)}$ is the solution operator to an initial value problem for an evolution equation (cf. [7]):

$$\left\{\begin{array}{rcl}[\partial_\alpha-\mathrm{i}P(\alpha,\tilde{\mathbf{x}},\partial_{\tilde{\mathbf{x}}})]w(\alpha,\tilde{\mathbf{x}}) &=& 0,\\ w(\alpha,\tilde{\mathbf{x}})|_{\alpha=\alpha_0} &=& w_0(\tilde{\mathbf{x}}),\end{array}\right. \tag{2.3}$$

where P is a pseudodifferential operator of order 1, and $w_0(\tilde{\mathbf{x}})$ is an set of CIGs obtained using an initial background velocity model, $c(\alpha_0)$. We use the shorthand notation, $\tilde{\mathbf{x}}=(\mathbf{x},\mathbf{p},z)$.

2.3. Geometric representation. Equation (2.3) describes how CIGs evolve under changing background models. Asymptotically, the wavefront set of w propagates according to a Hamiltonian flow, where the Hamiltonian is the principal symbol, P_1, of P. The corresponding rays are referred to as velocity rays. Equation (2.3) is a generalization (to arbitrary velocity perturbations) of the result given by S. Fomel (cf. [9]) who introduced the concept of velocity continuation and velocity rays for time migrated images.

The wavefront set of w can, in principle, be estimated from its representation in terms of wave packets or "curvelets". In [1] a frame of discrete, almost symmetric wave packets, φ_γ, is constructed, which we will use here; $\gamma=(j,\nu,k)$ with multi-index j representing translations in $\tilde{\mathbf{x}}$-space, ν denoting orientations, and k denoting the scale. A wave packet, essentially, looks like an oriented, "fat", localized plane wave. We have the transform pair,

$$w_0(\tilde{\mathbf{x}})=\sum_\gamma w_{0\gamma}\varphi_\gamma(\tilde{\mathbf{x}}),\quad w_{0\gamma}=\int\overline{\varphi_\gamma(\tilde{\mathbf{x}})}\,w_0(\tilde{\mathbf{x}})\,\mathrm{d}\tilde{\mathbf{x}}, \tag{2.4}$$

where $w_{0\gamma}$ are the wave-packet coefficients.

A construction and analysis of the solution of initial value problems of the type (2.3), using wave packets, is given in [1]. In this construction, an approximate solution is introduced that is based on decomposing the initial data into wave packets, φ_γ, according to (2.4), and subjecting the individual wave packets to a rigid motion derived from the Hamiltonian flow defined by P_1 (that is, the velocity rays in phase space) and initial values, $(\tilde{\mathbf{x}}_j,\nu\,2^k)$. A weak solution of the initial value problem is obtained by solving a Volterra integral equation the kernel of which is derived from this approximate solution.

To extract relevant information out of w_0, we need to obtain a sparse decomposition of the type (2.4):

$$w_0(\tilde{\mathbf{x}})\approx\sum_{m\in\{1,\ldots,M\}}w_{\gamma_m}\varphi_{\gamma_m}(\tilde{\mathbf{x}}), \tag{2.5}$$

with M minimal. Such a sparse decomposition can, for example, be obtained by methods of sparsity promoting optimization using ℓ^1 regularization (cf. [15]). We identify

$$(\mathbf{x}^{\gamma_m}, \mathbf{p}^{\gamma_m}, z^{\gamma_m}) = \tilde{\mathbf{x}}_{j_m}, \quad (\mathbf{k}_x^{\gamma_m}, \mathbf{k}_p^{\gamma_m}, k_z^{\gamma_m}) = 2^{k_m}\, \nu_m,\ m \in \{1, \ldots, M\}.$$

We note that $(\mathbf{k}_x^{\gamma_m}, z^{\gamma_m})$ provides information about the image dip, locally, at $(\mathbf{x}^{\gamma_m}, z^{\gamma_m})$ if k_m is sufficiently large.

3. Velocity estimation.

3.1. Optimization formulation - a geometric approach. An optimization approach to estimate the background velocity model using the angle transform was proposed in [3]. Here, we use an error criterion derived from this approach (cf. [19]) which has the appearance of a differential semblance [22]:

$$J(\alpha) = \|\partial_{\mathbf{p}} w(\alpha, ., ., .)\|^2_{(\mathbf{x},\mathbf{p},z)}, \quad w = \mathcal{A}_{we}(\alpha) d. \tag{3.1}$$

(In our notation, we suppress the presence of a deconvolution, ∂_t^{-1}, that should be applied to the data.) Through a composition with $\mathcal{A}_{we}^{-1}$, $\partial_{\mathbf{p}}$ generates annihilators of the data. We say that $\partial_{\mathbf{p}}$ maps a CIG to a "residual" CIG,

$$r(\alpha, \mathbf{x}, \mathbf{p}, z) = \partial_{\mathbf{p}} w(\alpha, \mathbf{x}, \mathbf{p}, z); \tag{3.2}$$

$r = 0$ if $c(\alpha)$ coincides with the "true" velocity model.

Returning to the wave packet decomposition of w_0, we now make use of the property that

$$\partial_{\mathbf{p}} \varphi_{\gamma_m} \approx \mathbf{k}_p^{\gamma_m} \varphi_{\gamma_m},$$

up to an error of $\mathcal{O}(2^{-k_m/2})$. Thus, the geometric counterpart of the residual gathers, $r(\alpha_0, \mathbf{x}, \mathbf{p}, z)$, becomes

$$r_g = \{\mathbf{k}_p^{\gamma_m}\}_{m=1,\ldots,M}. \tag{3.3}$$

The corresponding, geometric, error function is given by

$$J_g = \sum_{m \in \{1,\ldots,M\}} |\mathbf{k}_p^{\gamma_m}|^2. \tag{3.4}$$

Because, for sufficiently fine scales, in the "true" velocity model we obtain $\mathbf{k}_p^{\gamma_m} = \mathbf{0}$, we can view the elements of the set r_g as describing "residual angle dip (RAD)", expressed by the notation, $\mathbf{\Delta}_m = -\mathbf{k}_p^{\gamma_m}$, $m \in \{1, \ldots, M\}$.

3.2. A comparison with Residual Move Out. Instead of extracting (jointly, for all reflectors) $\{\mathbf{k}_p^{\gamma_m}\}_{m\in\{1,\ldots,M\}}$ for sufficiently fine scales, we could also have extracted subsets $\{(\mathbf{x}^{\gamma_m}, z^{\gamma_m}, \mathbf{p}^{\gamma_m})\}_{m\in N_r}$ pertaining to common reflectors labelled by r. Within each subset, we let $\mathbf{p}^{\gamma_{m_{r1}}}$ be distinct from $\mathbf{p}^{\gamma_{m_{r2}}}$, $m_{r1}, m_{r2} \in N_r$. We then arrive at a natural choice for an error function to estimate the background velocity,

$$\sum_r |z^{\gamma_{m_{r2}}} - z^{\gamma_{m_{r1}}}|^2, \tag{3.5}$$

which reflects the so-called residual moveout (RMO), [23, 16, 17]. (Instead of this differential RMO, one has also considered the curvature evaluated at $\mathbf{p} = \mathbf{0}$.)

The RMO evolution and RAD evolution with background velocity are illustrated in Fig. 1. Here, we consider the constant velocity case, that is, $c(\alpha)$ is independent of $(\mathbf{x}, z)$ for all α considered, and insert a horizontal reflector. (The "true" velocity was normalized to 1 km/s.) In Fig. 1,a) we show

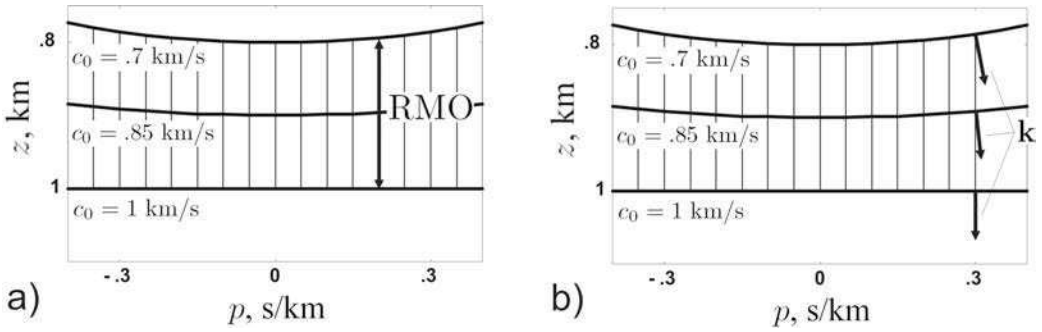

FIG. 1. *Background velocity continuation for the constant velocity case (the "true" velocity being $c_0 = 1$ km/s) and a horizontal reflector; a) depth RMO evolution (a horizontal gather corresponds to "true" velocity); b) RAD evolution (vertical orientation of* $\mathbf{k}$ *corresponds to "true" velocity).*

the RMO evolution starting from a velocity, $c(\alpha_0) = .7$ km/s, as the differential RMO (cf. (3.5)) tends to zero. In Fig. 1,b) we show the RAD evolution, again, starting from a velocity, $c(\alpha_0) = .7$ km/s, as the $\mathbf{p}$ components of $\mathbf{k}$ (cf. (3.4)) tend to zero.

Equation (3.5) measures only one component of the RMO, and, in general, all components should be accounted for. That is, $|\mathbf{x}^{\gamma_{m_{r2}}} - \mathbf{x}^{\gamma_{m_{r1}}}|^2$ needs to be included in the error function to obtain full sensitivity to changes in the background velocity. We illustrate this in Fig. 2. In Fig. 2,a) we show the constant velocity evolution of a CIG for a horizontal reflector, and in Fig. 2,b) we show the constant velocity evolution of a CIG for a dipping reflector. In the latter case, the RMO in $\mathbf{x}$ vs. $\mathbf{p}$ would yield a significant contribution to the full differential RMO error function.

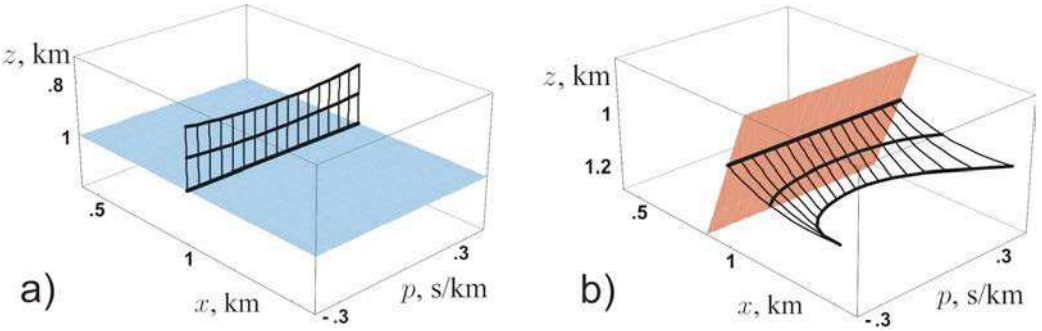

FIG. 2. *RMO evolution of common-image point gathers (thick horizontal line) with "true" velocity being $c_0 = 1$ km/s; a) the case of a horizontal (flat) reflector, yielding depth RMO; b) the case of a dipping (flat) reflector, yielding RMO in all directions.*

4. Sensitivity kernel - perturbation theory. We introduce the background model perturbation as a decomposition,

$$\delta s(\mathbf{x}, z) = \delta c(\mathbf{x}, z)^{-2} = \sum_{n=1}^{N} \delta s_n \, \psi_n(\mathbf{x}, z), \tag{4.1}$$

where the $\psi_n(\mathbf{x}, z)$ are smooth, and chosen appropriately in the sense that they represent the models under consideration in some optimal way. In the above, $s = c^{-2}$ represents model slowness squared. We assume that the model chosen in the application of the angle transform is sufficiently close to the "true" model, that is, δs represents a perturbation about the "true" model.

In the context of velocity continuation, we have $\delta s = -2c(\alpha_0)^{-3}\partial_\alpha c|_{\alpha=\alpha_0}\delta\alpha$ ($\delta\alpha = \alpha - \alpha_0$), where $c(\alpha_0)$ stands for the "true" model. We integrate the Hamilton system defined by the principal

symbol, P_1 (cf. (2.3)), backwards with initial data (at α) estimated from the CIGs. From the solution we extract $-\mathbf{k}_p^{\gamma_m}(\alpha_0;\alpha)$ which models $\mathbf{\Delta}_m$ if α_0 is the first value of the evolution parameter encountered where $\mathbf{k}_{\mathbf{p}}^{\gamma_m}$ becomes $\mathbf{0}$. In the context of optimization, we have modelled a "line search".

In this section, we use ray perturbation theory to obtain the Fréchet derivative of $\mathbf{k}_p^{\gamma_m}$. Invoking an adjoint state method, this Fréchet derivative determines a search "direction" in the space of slowness model perturbations. We note the similarities with linearized transmission tomography.

4.1. DSR ray perturbation. In preparation of constructing the Fréchet derivative of $\mathbf{k}_p^{\gamma_m}$, we summarize the perturbation of DSR rays underlying the geometry of the angle transform. The double-square root (DSR) equation has been introduced for data downward/upward continuation. The propagation of singularities by the solution of the DSR equation is considered in detail in [6]. The Hamiltonian for tracing DSR rays in phase space is given by

$$\mathcal{H}^{DSR}(z,\mathbf{x}_s,\mathbf{x}_r,k_z,\mathbf{k}_s,\mathbf{k}_r,\omega) = k_z - \sqrt{s(\mathbf{x}_s,z)\omega^2-|\mathbf{k}_s|^2} - \sqrt{s(\mathbf{x}_r,z)\omega^2-|\mathbf{k}_r|^2}; \tag{4.2}$$

the frequency, $\omega > 0$ while $z \in [0,Z]$, where Z denotes the maximum depth considered.

We consider perturbations of the background model in terms of s, with

$$s(\epsilon,\mathbf{x},z) = s_0(\mathbf{x},z) + \epsilon s_1(\mathbf{x},z). \tag{4.3}$$

Following [8] we expand the Hamiltonian according to

$$\mathcal{H}^{DSR} = \mathcal{H}_0^{DSR} + \epsilon\mathcal{H}_1^{DSR} + \dots \tag{4.4}$$

We have

$$\mathcal{H}_0^{DSR} = k_z - \sqrt{s_0(\mathbf{x}_s,z)\omega^2-|\mathbf{k}_s|^2} - \sqrt{s_0(\mathbf{x}_r,z)\omega^2-|\mathbf{k}_r|^2}, \tag{4.5}$$

$$\mathcal{H}_1^{DSR} = -\frac{1}{2}\left[\frac{s_1(\mathbf{x}_s,z)\omega^2}{\sqrt{s_0(\mathbf{x}_s,z)\omega^2-|\mathbf{k}_s|^2}} + \frac{s_1(\mathbf{x}_r,z)\omega^2}{\sqrt{s_0(\mathbf{x}_r,z)\omega^2-|\mathbf{k}_r|^2}}\right]. \tag{4.6}$$

In this section, we use the shorthand notation $\widetilde{\mathbf{x}} = (\mathbf{x}_s,\mathbf{x}_r,t)$ and $\widetilde{\mathbf{k}} = (\mathbf{k}_s,\mathbf{k}_r,\omega)$. The ray trajectories are expanded according to

$$\widetilde{\mathbf{x}}(z) = \widetilde{\mathbf{x}}_0(z) + \epsilon\widetilde{\mathbf{x}}_1(z) + \dots, \quad \widetilde{\mathbf{k}}(z) = \widetilde{\mathbf{k}}_0(z) + \epsilon\widetilde{\mathbf{k}}_1(z) + \dots, \tag{4.7}$$

where $(\widetilde{\mathbf{x}}_0(z;\widetilde{\mathbf{x}}^0,\widetilde{\mathbf{k}}^0),\widetilde{\mathbf{k}}_0(z;\widetilde{\mathbf{x}}^0,\widetilde{\mathbf{k}}^0))$, describe unperturbed DSR rays as solutions to the unperturbed Hamilton system,

$$\begin{aligned}
\frac{\mathrm{d}\widetilde{\mathbf{x}}_0}{\mathrm{d}z} &= \widetilde{\mathbf{v}}_1 = \frac{\partial\mathcal{H}_0^{DSR}}{\partial\widetilde{\mathbf{k}}},\ \widetilde{\mathbf{x}}_0(0) = \widetilde{\mathbf{x}}^0,\\
\frac{\mathrm{d}\widetilde{\mathbf{k}}_0}{\mathrm{d}z} &= \widetilde{\mathbf{v}}_2 = -\frac{\partial\mathcal{H}_0^{DSR}}{\partial\widetilde{\mathbf{x}}},\ \widetilde{\mathbf{k}}_0(0) = \widetilde{\mathbf{k}}^0.
\end{aligned} \tag{4.8}$$

We write $\widetilde{\mathbf{v}}_1 = (\mathbf{v}_{1s},\mathbf{v}_{1r},v_{1t})$, $\widetilde{\mathbf{v}}_2 = (\mathbf{v}_{2s},\mathbf{v}_{2r},v_{2t})$. DSR rays can be considered as curves in $(z,\mathbf{x}_s,\mathbf{x}_r,t)$ space. We also introduce the notation $\Gamma_0 = (\widetilde{\mathbf{x}}^0,\widetilde{\mathbf{k}}^0)$.

The first-order perturbations, $(\widetilde{\mathbf{x}}_1(z),\widetilde{\mathbf{k}}_1(z))$, satisfy the system of equations,

$$\begin{aligned}
\frac{\mathrm{d}\widetilde{\mathbf{x}}_1}{\mathrm{d}z} &= \left.\frac{\partial^2\mathcal{H}_0^{DSR}}{\partial\widetilde{\mathbf{k}}\partial\widetilde{\mathbf{x}}}\right|_{(\widetilde{\mathbf{x}}_0,\widetilde{\mathbf{k}}_0)}\cdot\widetilde{\mathbf{x}}_1 + \left.\frac{\partial^2\mathcal{H}_0^{DSR}}{\partial\widetilde{\mathbf{k}}\partial\widetilde{\mathbf{k}}}\right|_{(\widetilde{\mathbf{x}}_0,\widetilde{\mathbf{k}}_0)}\cdot\widetilde{\mathbf{k}}_1 + \left.\frac{\partial\mathcal{H}_1^{DSR}}{\partial\widetilde{\mathbf{k}}}\right|_{(\widetilde{\mathbf{x}}_0,\widetilde{\mathbf{k}}_0)},\ \widetilde{\mathbf{x}}_1(0) = 0,\\
\frac{\mathrm{d}\widetilde{\mathbf{k}}_1}{\mathrm{d}z} &= -\left.\frac{\partial^2\mathcal{H}_0^{DSR}}{\partial\widetilde{\mathbf{x}}\partial\widetilde{\mathbf{x}}}\right|_{(\widetilde{\mathbf{x}}_0,\widetilde{\mathbf{k}}_0)}\cdot\widetilde{\mathbf{x}}_1 - \left.\frac{\partial^2\mathcal{H}_0^{DSR}}{\partial\widetilde{\mathbf{x}}\partial\widetilde{\mathbf{k}}}\right|_{(\widetilde{\mathbf{x}}_0,\widetilde{\mathbf{k}}_0)}\cdot\widetilde{\mathbf{k}}_1 - \left.\frac{\partial\mathcal{H}_1^{DSR}}{\partial\widetilde{\mathbf{x}}}\right|_{(\widetilde{\mathbf{x}}_0,\widetilde{\mathbf{k}}_0)},\ \widetilde{\mathbf{k}}_1(0) = 0,
\end{aligned}$$

writing $\widetilde{\mathbf{x}}_1 = (\mathbf{x}_{1s},\mathbf{x}_{1r},t_1)$ and $\widetilde{\mathbf{k}}_1 = (\mathbf{k}_{1s},\mathbf{k}_{1r},\omega)$.

On the unperturbed DSR bicharacteristics, $\mathcal{H}_0^{DSR} = 0$, while $(\widetilde{\mathbf{x}}_1,\widetilde{\mathbf{k}}_1)$ satisfy the constraint,

$$\frac{\partial\mathcal{H}_0^{DSR}}{\partial\widetilde{\mathbf{x}}}\cdot\widetilde{\mathbf{x}}_1 + \frac{\partial\mathcal{H}_0^{DSR}}{\partial\widetilde{\mathbf{k}}}\cdot\widetilde{\mathbf{k}}_1 + \mathcal{H}_0^{DSR} = 0. \tag{4.9}$$

4.2. Geometry of the angle transform and perturbation of $\mathbf{k}_p^{\gamma_m}$. The DSR assumption, stating that rays are nowhere horizontal, implies that (two-way) travel time t depends monotonically on depth z. In the unperturbed (zero-order) situation, the geometry of the angle transform is recovered in the following manner. Given the initial values, Γ_0, equation (4.8) is solved yielding $(\mathbf{x}_{0s}(z,\Gamma_0),\mathbf{x}_{0r}(z,\Gamma_0),t_0(z,\Gamma_0)$ and $(\mathbf{k}_{0s}(z,\Gamma_0),\mathbf{k}_{0r}(z,\Gamma_0),\omega)$. Then, z_0 is determined by the constraint,

$$\omega^{-1}\,\langle\tfrac{1}{2}(\mathbf{k}_{0s}(z_0,\Gamma_0)-\mathbf{k}_{0r}(z_0,\Gamma_0)),\mathbf{x}_{0r}(z_0,\Gamma_0)-\mathbf{x}_{0s}(z_0,\Gamma_0)\rangle = t_0(z_0,\Gamma_0), \tag{4.10}$$

see [6] for details. Substituting this z_0, we obtain

$$\begin{array}{rclcrcl} \mathbf{x}_0 &=& \tfrac{1}{2}(\mathbf{x}_{0s}+\mathbf{x}_{0r}) &,& \mathbf{k}_{0x} &=& \mathbf{k}_{0s}+\mathbf{k}_{0r},\\ \mathbf{p}_0 &=& \tfrac{1}{2\omega}(\mathbf{k}_{0s}-\mathbf{k}_{0r}) &,& \mathbf{k}_{0p} &=& \omega(\mathbf{x}_{0r}-\mathbf{x}_{0s}) \end{array} \tag{4.11}$$

giving a map from Γ_0 to $(\mathbf{x}_0,\mathbf{p}_0,z_0,\mathbf{k}_{0z},\mathbf{k}_{0p},k_{0z})$ with $k_{0z}=\Theta(z_0,\mathbf{x}_{0s},\mathbf{x}_{0r},\mathbf{k}_{0s},\mathbf{k}_{0r},\omega)$. Here $\Theta:\omega\rightarrow k_z$, for given $(z,\mathbf{x}_s,\mathbf{x}_r,\mathbf{k}_s,\mathbf{k}_r)$, solves the equation,

$$\mathcal{H}^{DSR}(z,\mathbf{x}_s,\mathbf{x}_r,\Theta(z,\mathbf{x}_s,\mathbf{x}_r,\mathbf{k}_s,\mathbf{k}_r,\omega),\mathbf{k}_s,\mathbf{k}_r,\omega)=0 \tag{4.12}$$

[20, Lemma 4.1]; this mapping has an inverse, $\Theta^{-1}:\ k_z\rightarrow\omega$.

Upon perturbing the DSR rays, equation (4.10) is satisfied by $z_0+\epsilon z_1+\ldots$ replacing z_0, with

$$z_1=\frac{\langle\tfrac{1}{2}(\mathbf{k}_{1s}-\mathbf{k}_{1r}),\mathbf{x}_{0r}-\mathbf{x}_{0s}\rangle+\langle\tfrac{1}{2}(\mathbf{k}_{0s}-\mathbf{k}_{0r}),\mathbf{x}_{1r}-\mathbf{x}_{1s}\rangle}{\omega v_{1t}-[\langle\tfrac{1}{2}(\mathbf{v}_{2s}-\mathbf{v}_{2r}),\mathbf{x}_{0r}-\mathbf{x}_{0s}\rangle+\langle\tfrac{1}{2}(\mathbf{k}_{0s}-\mathbf{k}_{0r}),\mathbf{v}_{1r}-\mathbf{v}_{1s}\rangle]} \tag{4.13}$$

all evaluated at (z_0,Γ_0). We then expand $\mathbf{k}_p=\mathbf{k}_{0p}+\epsilon\mathbf{k}_{1p}+\ldots$, with

$$\mathbf{k}_{1p}=\omega\,[\mathbf{x}_{1r}(z_0,\Gamma_0)+z_1\,\mathbf{v}_{1r}(z_0,\Gamma_0)-\mathbf{x}_{1s}(z_0,\Gamma_0)-z_1\,\mathbf{v}_{1s}(z_0,\Gamma_0)]. \tag{4.14}$$

This equation provides the Fréchet derivative of $\mathbf{k}_p$ with respect to a model perturbation of "strength" ϵ. Through the presence of $\mathbf{x}_{1s}$, $\mathbf{x}_{1r}$, and also of $\mathbf{k}_{1s}$, $\mathbf{k}_{1r}$, we note the relation with the geodesic X-ray transform for transmission tomography.

In the application, we estimate $(\mathbf{x}_0,\mathbf{p}_0,z_0,\mathbf{k}_{0z},\mathbf{k}_{0p},k_{0z})$ from the CIGs, but using the geometry of the angle transform, these provide Γ_0.

REFERENCES

[1] F. Andersson, M.V. de Hoop, H.F. Smith, and G. Uhlmann, *A multi-scale approach to hyperbolic evolution equations with limited smoothness*, Communications in Partial Differential Equations, in print (2008).

[2] E.J. Candés, L. Demanet, D. Donoho, and L. Ying, *Fast discrete curvelet transforms*, SIAM Multiscale Model. Simul., 5 (3) (2006), pp. 861–899.

[3] M.V. de Hoop, R.D. van der Hilst, and P. Shen, *Wave-equation reflection tomography: Annihilators and sensitivity kernels*, Geoph. J. Int., 167 (2006), pp. 1332–1352.

[4] H. Douma and M.V. de Hoop, *Explicit expressions for pre-stack map time-migration in isotropic and VTI media and the applicability of map depth-migration in heterogeneous anisotropic media*, Geophysics, 71 (2006), pp. S13–S28.

[5] ———, *Leading-order seismic imaging using curvelets*, Geophysics, 72 (2007), pp. S231–S248.

[6] A.A. Duchkov and M.V. de Hoop, *Velocity continuation in the downward continuation approach to seismic imaging*, J. Geoph. Int., in print (2008).

[7] A.A. Duchkov, M.V. de Hoop, and A. Sá Barreto, *Evolution-equation approach to seismic image, and data, continuation*, Wave Motion, 45 (2008), pp. 952–969.

[8] V. Farra, *Computation of second-order traveltime perturbation by hamiltonian ray theory*, Geophys. J. Int., 136 (1999), pp. 205–217.

[9] S. Fomel, *Velocity continuation and the anatomy of residual prestack time migration*, Geophysics, 68 (2003), pp. 1650–1661.

[10] S.V. Goldin, *Geometric fundamentals of seismic imaging: A geometric theory of the upper level*, in Amplitude-preserving seismic reflection imaging, London, 1998, Proceedings of the Workshop, Geophysical Press, pp. 120–223.

[11] ———, *Geometrical fundamentals of seismic imaging: realization of contact mappings*, Sib. Journ. Num. Math., 6(4) (2003), pp. 323–345.
[12] F. Herrmann, G. Hennenfent, and P. Moghaddam, *Seismic imaging and processing with curvelets*, Extended Abstracts, EAGE 69th Annual Meeting, (2007).
[13] B. Hua and G. A. McMechan, *Parsimonious 2D prestack Kirchhoff depth migration*, Geophysics, 68 (2003), pp. 1043–1051.
[14] E. Iversen and H. Gjostdal, *Event-oriented velocity estimation based on prestack data in time or depth domain*, Geoph. Prosp., 44 (1996), pp. 643–686.
[15] I. Loris, G. Nolet, I. Daubechies, and F.A. Dahlen, *Tomographic inversion using ℓ^1-norm regularization of wavelet coefficients*, Geophys. J. Int., 170 (2007), pp. 359–370.
[16] P.C. Sava and B. Biondi, *Wave-equation migration velocity analysis –I: Theory*, Geophysical Prospecting, 52 (2004), pp. 593–606.
[17] P.C. Sava and S. Fomel, *Time-shift imaging condition in seismic migration*, Geophysics, 71(6) (2006), pp. S209–S217.
[18] H.F. Smith, *A Hardy space for Fourier integral operators*, Jour. Geom. Anal., 8 (1998), pp. 629–654.
[19] C.C. Stolk and M.V. De Hoop, *Seismic inverse scattering in the 'wave-equation' approach*, MSRI preprint, #2001–047 (2001).
[20] ———, *Modeling of seismic data in the downward continuation approach*, SIAM J. Appl. Math., 65 (2005), pp. 1388–1406.
[21] ———, *Seismic inverse scattering in the downward continuation approach*, Wave Motion, 43 (2006), pp. 579–598.
[22] W.W. Symes and J. Carazzone, *Velocity inversion by differential semblance optimization*, Geophysics, 56 (1991), pp. 654–663.
[23] X.B. Xie and H. Yang, *The finite-frequency sensitivity kernel for migration residual moveout and its applications in migration velocity analysis*, Geophysics, 73(6) (2008), pp. S241–S249.